Progression of human breast cancers to the metastatic state is linked to hydroxyl radical-induced DNA damage

(cancer etiology/tumor metastasis/DNA base damage/free radicals/malignant cancer markers)

DONALD C. MALINS*, NAYAK L. POLISSAR†, AND SANDRA J. GUNSELMAN*

*Molecular Epidemiology Program, Pacific Northwest Research Foundation, Seattle, WA 98122; and †The Mountain-Whisper-Light Statistical Consulting, Seattle, WA 98112 and the Department of Biostatistics, University of Washington, Seattle, WA 98195

ABSTRACT   Hydroxyl radical damage in metastatic tumor DNA was elucidated in women with breast cancer, and a comparison was made with nonmetastatic tumor DNA. The damage was identified by using statistical models of modified base and Fourier transform-infrared spectral data. The modified base models revealed a greater than 2-fold increase in hydroxyl radical damage in the metastatic tumor DNA compared with the nonmetastatic tumor DNA. The metastatic tumor DNA also exhibited substantially greater base diversity than the nonmetastatic DNA, and a progression of radical-induced base damage was found to be associated with the growth of metastatic tumors. A three-dimensional plot of principal components from factor analysis, derived from infrared spectral data, also showed that the metastatic tumor DNA was substantially more diverse than the tightly grouped nonmetastatic tumor DNA. These cohesive, independently derived findings suggest that the hydroxyl radical generates DNA phenotypes with various metastatic potentials that likely contribute to the diverse physiological properties and heterogeneity characteristic of metastatic cell populations.

Metastasis of tumors is a major cause of treatment failure in cancer patients. It is a complex process involving the detachment of cells from the primary neoplasm, their entrance into the circulation, and the eventual colonization of local and distant tissue sites (1). Metastatic cells are characterized by substantial heterogeneity and diverse physiological properties (1, 2). Oxidative stress has been implicated as an important factor in metastasis, notably because it results in a loss of cell adhesion which is the prerequisite for cellular detachment and host tissue invasion (1, 3). Oxidative stress, which is rapidly induced in murine mammary tumor cells exposed to sublethal (nontoxic) concentrations of H_2O_2, inhibited tumor cell attachment to immobilized laminin and fibronectin (3). Moreover, pretreatment of tumor cells with H_2O_2 and H_2O_2-generating systems prior to intravenous injection of the cells enhanced experimental lung tumor colony formation (3). Thus, treatments that favored reactive oxygen species also inhibited tumor attachments to extracellular proteins in vitro and enhanced experimental metastasis in vivo. This is consistent with evidence showing that oxidative stress enhances cell invasion into local host tissue (1, 2) and that hydroxyurea-treated melanoma cells become transiently more metastatic and develop a resistance to H_2O_2 toxicity (4).

The suspected role of H_2O_2 in metastasis is a logical extension of an interest in the propensity for reactive oxygen species to induce cancer-related damage in DNA. Primarily, the focus has been on damage inflicted by the highly reactive hydroxyl radical (·OH) on the nucleotide bases (5, 6). The Fe^{2+}-catalyzed conversion of H_2O_2 is a major route to the

synthesis of the ·OH in living systems (7, 8). The source of H_2O_2 has been suggested to be the redox cycling of estrogens (9–12) and xenoestrogens (13–15). Notably, metabolic redox cycling between 4-hydroxyestradiol and its quinone has been shown to generate ·OH-induced DNA base damage in vitro (12). Progressive increases in the radical attack on the DNA result in mutagenic structures, such as 8-hydroxyadenine (8-OH-Ade) (16) and 8-hydroxyguanine (8-OH-Gua) (17, 18), that are associated with a heightened risk of cancer. An additional component of the radical attack is the introduction of putatively nonmutagenic structures into DNA—the ring-opened (Fapy) derivatives of adenine and guanine (19–24). The ratio of Fapy structure to OH-adduct is likely governed by the 8-oxyl intermediate, a carbon-centered radical formed from the initial reaction of the ·OH with adenine (A8OH·) or guanine (G8OH·) (24, 25). The radical intermediate is "redox ambivalent," implying that a shift in the redox status of DNA alters the relative rates of formation of the Fapy structures and OH-adducts. The former structures would be favored under reductive conditions, and the latter under oxidative conditions. The chemical transformations likely responsible for the formation of these structures are depicted in Fig. 1. The Fapy structure blocks DNA synthesis (26) and mRNA transcription (27), whereas OH-adducts induce misincorporation (18, 26). Thus, under conditions of ·OH stress, the accumulation of Fapy structures in the DNA apparently represents a favorable alternative to the acquisition of the OH-adducts (5, 24).

DNA is ideally suited to the formation of the redox-mediated base modifications in that H^+, e^-, and H_2O (Fig. 2) are readily available within the DNA matrix. Moreover, electron transfer from base to base along the helix axis is extremely rapid (estimated at $10^{14} sec^{-1}$) (28) and can extend to 100 base pairs (25). Proton transfer perpendicular to the helix axis involves only a slight displacement of the equilibrium position of the bridging proton and is similarly an extremely fast process (25). Repair enzymes—e.g., glycosylases—are known to repair the Fapy structure (19–23, 29) and the OH-adducts at similar rates (19–21). Additionally, the Fapy structure may revert to the original base via the action of purine imidazole cyclase (30). Overall, the DNA damage is a function of the rate of base modification and repair (5, 24, 29); however, the repair capacity appears to be significantly reduced in tumors (31).
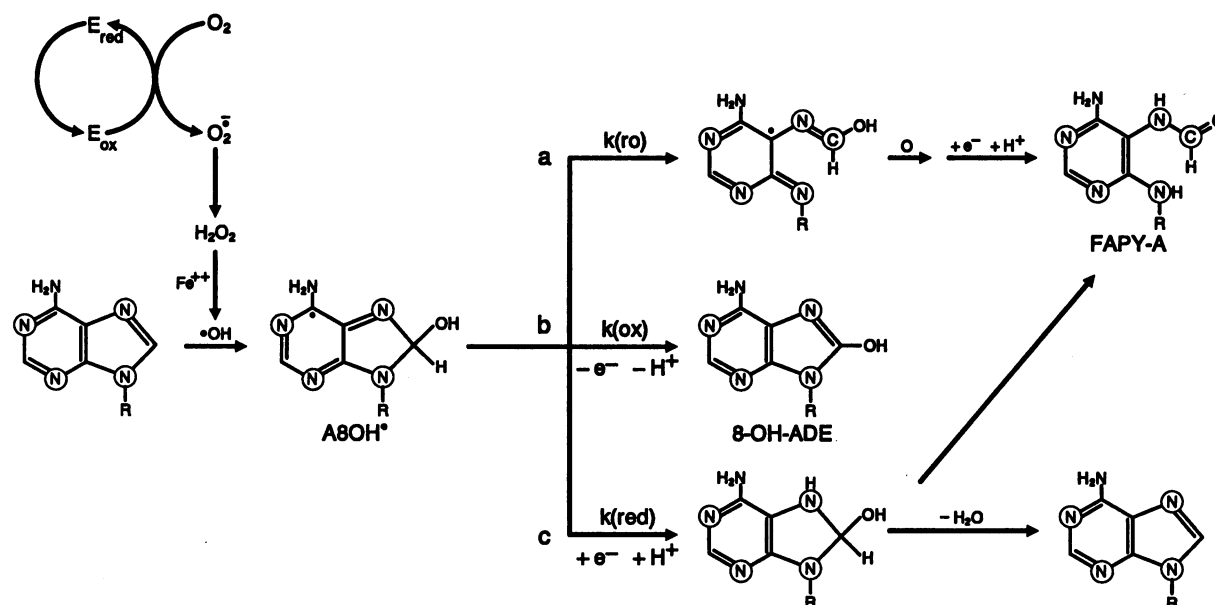
FIG. 1. Proposed scheme for the formation of Fapy derivatives and OH-adducts in the female breast (24, 25). H_2O_2, formed from the redox cycling of estrogens and/or xenoestrogens (E), is converted to the ·OH in the presence of catalytic concentrations of Fe^{2+}. The ·OH attacks the base (adenine), forming the redox ambivalent 8-oxyl intermediate (A8OH·). A shift in the redox status of the DNA favoring reductive pathways (a and c) leads to the Fapy structure, whereas a shift in favor of oxidation (b) results in the formation of the mutagenic OH-adduct (8-OH-Ade). A reversion to the original base is possible as shown in the dehydration reaction (c). [Adapted with permission from ref. 25 (copyright 1989 American Chemical Society).]

A prime example of the damaging effects of the ·OH on DNA was found in the cancerous[‡] and noncancerous human breast in which substantial damage to the base structure of DNA (often exceeding one modified base for every 10^4 equivalent normal bases) was revealed by gas chromatography-mass spectrometry (GC-MS) (24). The damaged bases included the mutagens 8-OH-Gua and 8-OH-Ade and the ring-opened products 2,6-diamino-4-hydroxy-5-formamidopyrimidine [Fapyguanine (Fapy-G)] and 4,6-diamino-5-formamidopyrimidine [Fapyadenine (Fapy-A)]. DNA from the noncancerous breast was characterized by a high ratio of Fapy-A to 8-OH-Ade and 8-OH-Gua. However, a dramatic shift in this relationship in favor of OH-adducts was found in the cancerous breast. This alteration in the modified base relationships was attributed primarily to a shift in the redox status of the cells favoring oxidative conversions from the 8-oxyl derivative (ref. 24; Fig. 1).

A notable feature of previously reported plots of predicted cancer probability vs. the log_{10} ratio of Fapy structures to OH-adducts (24) and predicted cancer probability vs. the risk score derived from Fourier transform-infrared (FT-IR) spectral data (32) was the sharp rate of change reflected in the sigmoid curves. This suggested that a slight change in redox status, such as initiated by an increase in the ·OH, would result in a relatively large change in the cancer probability. Both statistical relationships reflect the nonrandom, cancer-related progression of damage identified in the breast DNA of normal women (24, 32). We now refer to this nonrandom progression of damage as radical-induced DNA disorder (RIDD).

The keen interest in the nature of metastasis has focused to a considerable extent on alterations in cellular morphology and physiology (33, 34) to the virtual exclusion of potentially critical events in the microenvironment of DNA that damage the molecular structure and potentially give rise to cellular changes known to characterize the development and progression of metastatic tumors. However, recent advances in analytical techniques (24, 32) have substantially enhanced the ability to elucidate subtle cancer-related changes in DNA (35).

The successful use of the complementary techniques of GC-MS and FT-IR spectroscopy in this regard (24, 32) led to the application of these powerful capabilities to increase
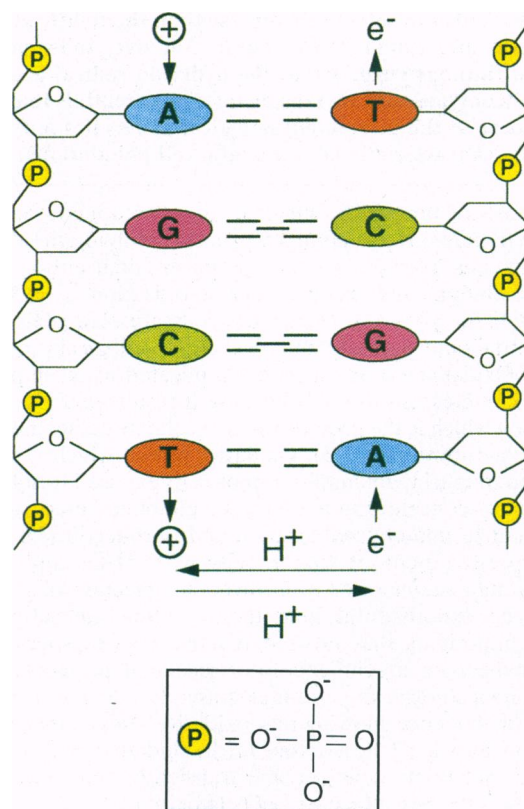

FIG. 2. Proton and electron transfer in DNA. Electron transfer occurs horizontally and proton transfer perpendicularly to the helix axis. The redox status is dependent on the balance between H^+, e^-, and H_2O (25) once the ·OH attacks a base and introduces the redox ambivalent 8-oxyl derivative (A8OH·; see Fig. 1). [Adapted with permission from ref. 25 (copyright 1989 American Chemical Society).]

[‡]No distinction was made with respect to the presence or absence of positive subaxillary lymph nodes.

understanding of important molecular changes associated with metastasis in the female breast.

Hydroxyl radical damage in DNA was studied in women with invasive ductal carcinoma of the breast, with and without evidence for metastasis (positive subaxillary lymph nodes), and compared with DNA from noncancerous tissue. Using previously employed Fapy-A/8-OH-Ade statistical models (24), we analyzed the DNA of metastatic tumors (IDC_m) and compared it to the DNA of nonmetastatic tumors (IDC). Comparisons were also made between statistical models of FT-IR spectral profiles of IDC_m, IDC, and DNA from reduction mammoplasty tissue (RMT) by using principal components analysis (PCA).

MATERIALS AND METHODS

Tissue Acquisition and DNA Isolation. Tissues were obtained from local Seattle hospitals and The Cooperative Human Tissue Network (Cleveland). A total of 12 tissues were obtained from 12 patients with invasive ductal carcinoma of the breast with no lymph node involvement, of which one was multifocal (the second focus being a signet ring cell carcinoma, which was not evaluated) and one was bilateral breast cancer (only one of which was evaluated). A total of 25 tissues were obtained from 25 patients with invasive ductal carcinoma having one or more lymph nodes positive for metastatic cancer. No unusual histologies were evident among the nonmetastatic and metastatic groups with the exception of the two IDC samples mentioned. Tumor size was based on the maximum dimension of the tumor, as recorded in the pathology reports. Noncancerous breast tissue was obtained from 21 patients who had undergone hypermastia surgery (reduction mammoplasty). Routine pathology showed no cellular changes other than occasional nonneoplastic—e.g., fibrocystic—lesions in these tissues.

After excision, each tissue was flash frozen in liquid nitrogen and stored at $-80°C$. DNA was isolated from the tissues as described (36), dissolved in deionized water, and aliquoted for GC-MS ($\approx 50\ \mu g$ of DNA was analyzed in duplicate for a total of 100 μg) and FT-IR spectroscopy ($\approx 20\ \mu g$), as reported (24, 32). Each DNA sample was completely dried by lyophilization, purged with pure nitrogen, and stored in an evacuated, sealed glass vial at $-80°C$ (32). All samples were analyzed by FT-IR spectroscopy. The total amount of DNA available made it possible to analyze nine IDC_m and six IDC samples by GC-MS.

GC-MS and FT-IR Spectroscopic Analysis. The $\approx 50\ \mu g$ of DNA was hydrolyzed, derivatized, and analyzed by GC-MS as described (24, 37). The GC-MS data were expressed in nmol of base lesion per mg of DNA. The IR spectra were obtained by using the Perkin-Elmer System 2000 equipped with an I-series microscope (Perkin–Elmer). Each spectrum was specified by the absorbance at each integer wavenumber from 2000 to 700 cm^{-1}. Only the interval from 1750 to 700 cm^{-1}, which included all major variations among spectra, was included in this analysis. A baseline adjustment and normalization was carried out as reported (32). One RMT was represented by two sections. The mean of the two adjusted and normalized spectra was used in these analyses. The multiplicative normalizing factor was applied to absorbances between 1750 and 700 cm^{-1}. By using deuterium exchange (38), no evidence was found to suggest that absorbed moisture contributed to the spectral properties of DNA.

Statistical Analysis. IDC_m and IDC were compared by using the *t* test on the following statistical models: log_{10}(Fapy-A), log_{10}(8-OH-Ade), log_{10}(Fapy-A + 8-OH-Ade), and log_{10}(Fapy-A/8-OH-Ade). Log_{10} data were used to produce a more normal distribution. The association of base concentration statistics with tumor size was measured using the Pearson correlation coefficient and simple linear regression.

PCA is a statistical procedure applied to a single set of variables with the aim of discovering a few variables (components) that are independent of each other and which capture most of the

information in the original, long list of variables. The methodology can greatly reduce the number of variables of concern. PCA partitions the total variance by finding the first principal component (PC) (a linear combination of the variables) which accounts for the maximum amount of variance. PCA then finds a second combination, independent of the first PC, such that it accounts for the next largest amount of variance. This procedure continues until a number of independent PCs are found that explain a significant portion of the total variance. In the present context, PCA was a way to identify major features of absorbance-wavenumber variation across a collection of spectra and describe that variation succinctly.

By using PCA, it is possible to identify a small number of components that serve as "building blocks" for the spectra, so that each spectrum can be represented by a few PC scores. PCA was carried out with the grand mean spectrum subtracted from individual spectra. Prior to the analysis, it was decided to retain enough components to explain at least 90% of the total variation (around the mean) of the data set. To determine if some of the differences among spectra might be due to age, the correlation between age and each PC score was calculated. To visualize the spectral relationship of the cancer and noncancer groups (IDC_m, IDC, and RMT), plots were constructed based on their first three PC scores.

RESULTS

Nucleotide Base Measurements. The mean log_{10} modified base values given in Fig. 3 differ significantly ($P = 0.05$ and 0.06) in favor of the IDC_m, representing a 2.3- and 2.4-fold increase over the IDC. In addition, the IDC_m show greater variation (diversity) than the IDC, as demonstrated by the standard deviations of base concentration statistics. The standard deviation is approximately twice as large in the IDC_m group than in the IDC group for both the log_{10}(8-OH-Ade) and log_{10}(Fapy-A + 8-OH-Ade) concentrations.

The greater diversity of the IDC_m appears to be related to the progression of the metastatic process (Fig. 4). The values for the IDC_m are distinctly more dispersed than those for the IDC. The regression line for the IDC_m is steeper (with Pearson correlation coefficient of $r = 0.75$; $P = 0.02$) than for the IDC ($r = 0.53$; $P = 0.3$) in relation to tumor size, although the difference in slopes and correlations is not statistically significant ($P = 0.2$, based on F from multiple regression). The slope in the IDC group is 0.020 (SD = 0.016), indicating an $\approx 5\%$ multiplicative increase in ratio per 1-cm increase in tumor size for the IDC group. For the IDC_m group, the slope is 0.108 (SD = 0.036) indicating a 28% increase in the ratio per 1-cm
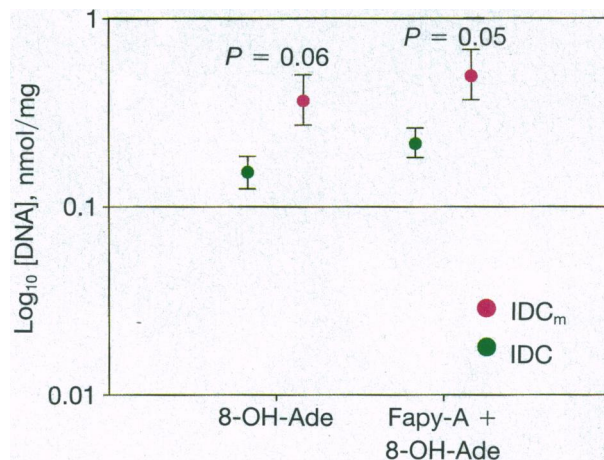

FIG. 3. A plot showing the mean concentrations ± SEM of two different modified base models in relation to the IDC_m and IDC. The difference between the IDC_m and the IDC in relation to mean log_{10}(Fapy-A) and mean log_{10}(Fapy-A/8-OH-Ade) values was not statistically significant.
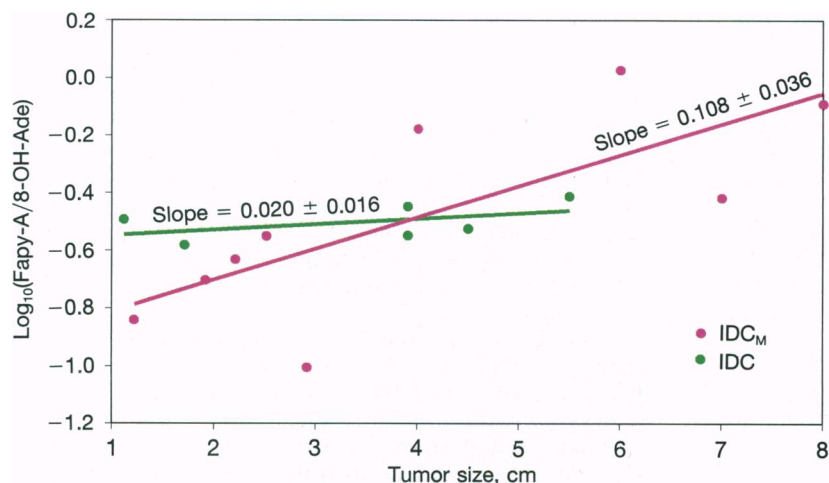
FIG. 4. Plot showing the $\log_{10}$(Fapy-A/8-OH-Ade) for the IDC_m and IDC vs. the size of the metastatic and nonmetastatic tumors. Statistical analysis showed that the regression line for the IDC_m is steeper, and the greater dispersion of values around the line indicates substantially increased diversity.

increase in tumor size. The variability around the regression lines is also significantly different between the IDC_m and IDC, as indicated by the standard deviation of the estimate: 0.247 for the IDC_m and 0.060 for the IDC group, a ratio of four ($P = 0.01$; F test). One outlier in the $\log_{10}$ ratio was removed from the analysis. This IDC had a $\log_{10}$ ratio of 0.07, distinctly an outlier compared with the range for the six other IDC samples of -0.4 to -0.6, with a mean of -0.5 and a standard deviation of 0.06. The outlier was nine standard deviations from the mean of the remaining IDC samples. There were no statistically significant correlations between base concentrations and age and the number and percentage of positive lymph nodes. Similarly, there were no statistically significant associations between tumor size, age, and the number or percentage of positive lymph nodes.

PCA of Spectral Profiles. Spectral profiles revealed great diversity of the IDC_m group and homogeneity of the IDC group. Fig. 5 shows a three-dimensional representation of the spectra based on PCA. The position in this plot is determined by the absorbance spectrum, mainly expressed as the height, width, and location of peaks. There is a core cluster of IDC samples

in the upper part of the plot (indicated by yellow spheres). The two IDC samples in the lower left part of the plot are outliers well removed from the core cluster. Notably, these are (*i*) an IDC with a second focus of signet ring cell carcinoma and (*ii*) a bilateral breast cancer. As apparent from the plot, both the IDC_m cluster (magenta) and the RMT cluster (blue) are considerably larger—indicating greater spectral diversity—than the core IDC cluster. The substantial spectral diversity in the RMT is consistent with the previously reported pronounced diversity in DNA of noncancerous breast tissue (32).

The size of a cluster can be measured and its spectral diversity represented by the mean distance of the members from the centroid of the cluster. This distance can be expressed as an approximate percent difference in normalized absorbance per wavenumber between a cluster member and the mean spectrum for the cluster, which lies at its centroid. The distance expressed as a percent difference is calculated as (*i*) 100% times the square root of the mean squared difference in normalized absorbance across wavenumbers 1750 to 700 cm^{-1}, which is then (*ii*) divided by 1.0, the approximate mean normalized absorbance for most spectra. For the comparison
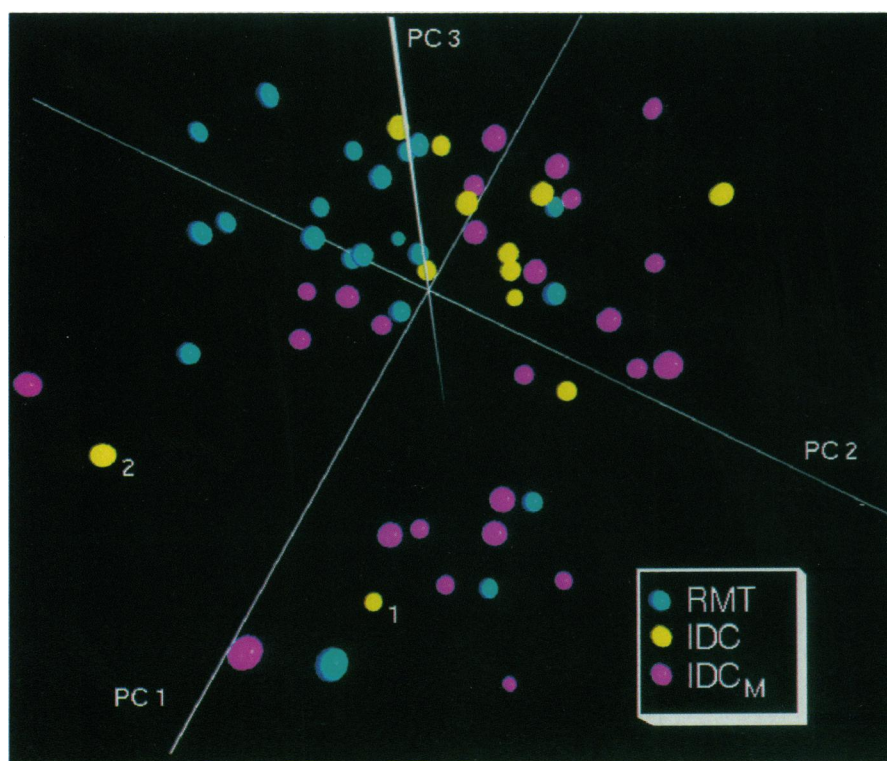

FIG. 5. A three-dimensional plot of PC 1, 2 and 3. Each sphere represents a DNA absorbance spectrum. The location of a sphere is determined by the "shape" of the spectrum, including height, width, and location of absorbance peaks. The core cluster of IDC spheres in the upper part of the plot (yellow) is significantly smaller than the more diverse and larger IDC_m cluster (magenta). The RMT and IDC_m clusters substantially overlap and the difference in size is not statistically significant. Outliers "1" and "2" represent a multifocal carcinoma, with one focus being a highly malignant signet ring cell carcinoma and the other being a bilateral breast cancer, respectively.
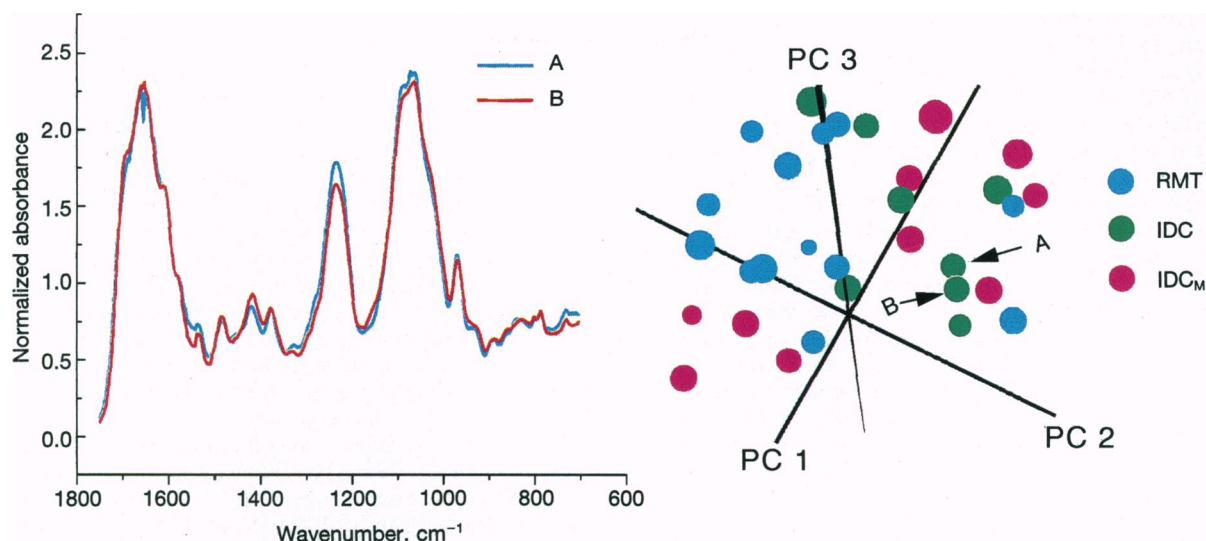
FIG. 6.   Two IDC spectra are shown which are spatially close on the adjacent three-dimensional PC plot (see arrows marked A and B). The two overlaid spectra differ by a mean of only 3% in normalized absorbance, demonstrating the high precision of the PCA and the fact that spatially close spheres have almost identical spectral profiles.

of cluster sizes, three RMT, three IDC_m and two IDC samples that lie at outlier distances from the centroid in each group were removed to define a core cluster for the RMT, IDC_m, and IDC. All outliers had at least a 20% difference from any member of their cluster. On the basis of centroids and distances of the remaining cases, the spectral diversity (mean distance from the centroid) was 12.4% for the IDC_m group, 7.3% for the IDC group, and 9.2% for the RMT group. An approximate P value for the difference in diversity between groups was based on the Mann–Whitney test, comparing distances to the centroids without outliers: $P = 0.003$ for IDC vs. IDC_m; $P = 0.04$ for RMT vs. IDC_m; and $P = 0.4$ for RMT vs. IDC. (The P values are approximate because dependence among distances is introduced through the calculation of the common centroid.)

Based on initial PCA of the 58 samples (RMT, $n = 21$; $IDC_m, n = 25$; and IDC, $n = 12$), four outliers were detected—specimens whose FT-IR spectra departed strikingly from the rest of the group and which had outlier PC scores. The PCA was repeated, initially eliminating these four outliers. The PC scores were then calculated for these outliers in a manner similar to the others (subtracting the grand mean spectrum of the

54 samples and then projecting each of the residual spectra on the PC eigenvectors). It was found that 91% of the variation in absorbance of the 54 samples was explained by the first five components. This implies that variation among spectra is highly structured. The 1051 wavenumbers from 1750 to 700 cm^{-1} constitute potentially 1051 dimensions of variation. Over 90% of this variation can be represented by only five dimensions.

There were only weak correlations of PC scores with age, but some correlations were statistically significant for all samples combined. Correlations between age and PC scores were as follows: $r = 0.21$ for component 1 and age ($P = 0.1$), $r = 0.29$ for component 2 and age ($P = 0.003$), $r = 0.03$ for component 3 and age ($P = 0.8$), $r = 0.25$ for component 4 and age ($P = 0.06$), and $r = 0.30$ for component 5 and age ($P = 0.02$). The small magnitude of these correlations suggests very little influence of age on spectral structure. Further, even the statistically significant correlations (PC 2 and PC 5) appear to be an artifact because correlations between the PC scores and age in the cancer and noncancer groups separately are very weak (less than ±0.18) and are not significant (minimum $P = 0.4$). There is a broad range of ages for all groups, which should allow a substantial true correlation to be detected: 17–89 years
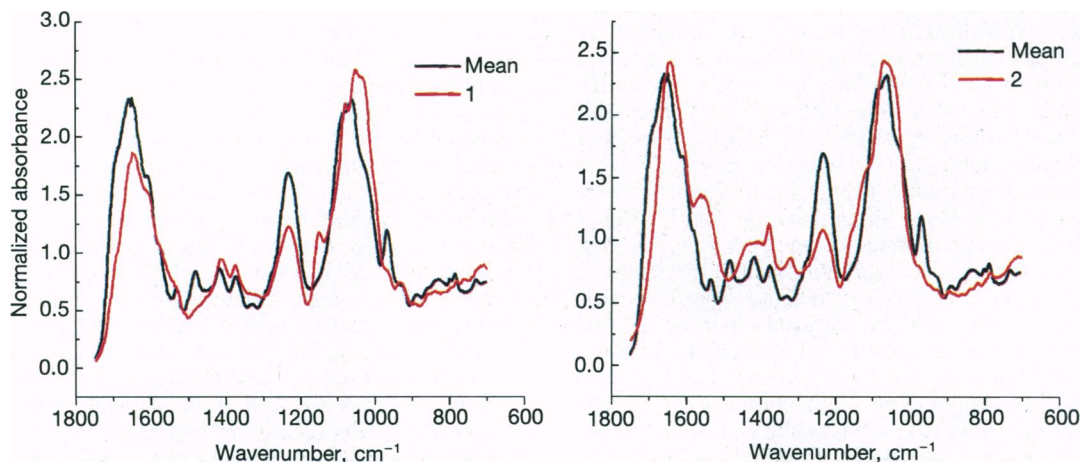

FIG. 7.   Spectral profiles of two IDC outliers (see Fig. 5) compared with the spectral profile of the mean IDC core cluster; "1" represents a multifocal carcinoma, with one focus being a highly malignant signet ring cell carcinoma, and "2" represents a bilateral breast cancer. In each case, the dramatic difference between the mean and outlier spectrum is apparent over most of the spectral region (see text for wavenumber–structure relationships) illustrating the pronounced structural discrimination associated with the PCA.

for all samples, 26–89 years for cancer (IDC_m and IDC), and 17–63 years for RMT. There was also no statistically significant correlation of the PC scores with the number or percentage of positive lymph nodes.

Fig. 6 depicts two overlaid spectra that lie close together on the three-dimensional PC plot together with their location on the plot. The actual spectra differ by a mean of only 3% in normalized absorbance, indicating high precision in characterizing spectral phenotypes. The two IDC outliers mentioned earlier are also distinct in spectral profile from the core IDC cluster. Fig. 7 shows these two spectra superimposed on the mean normalized spectrum of the IDC core cluster. Differences are notable over most of the spectral area but especially in the following regions: 1700 to 1350 cm^{-1}, the peak at $\approx$1240 cm^{-1}, and 1180 to 900 cm^{-1}. These regions generally represent N—H and C—O vibrations of the bases, PO_2 antisymmetric stretching vibrations of phosphodiester groups, and C—O vibrations of deoxyribose, respectively (32, 39).

DISCUSSION

The etiology of metastasis is poorly understood and specific markers of the transformation process have not been identified, although several studies have suggested that structural and functional alterations in genes may play a role (1, 40–42). Metastatic cell populations are characterized by pronounced heterogeneity and diverse physiological properties (1, 2). They exhibit a wide range of genetic, biochemical, immunological, and other characteristics that facilitate the invasion and colonization of host tissues (1, 2). However, virtually no prior information was available on alterations in DNA specifically relating to metastasis, such as may arise from free radicals. Yet these highly reactive substances have been linked to the formation of a broad range of mutagenic OH-adducts and putatively nonmutagenic Fapy structures in cancerous and noncancerous breast tissues (24, 43, 44). Accordingly, we hypothesized that the type of radical reactions previously shown to be associated with DNA damage and cancer (24, 32) would, once a tumor develops, impose additional damage that gives rise to the unique properties associated with metastatic cell populations (1, 2).

The role played by the ·OH in metastasis was examined by using the powerful complementary techniques of GC-MS and FT-IR spectroscopy. The ready availability of H$^+$, e$^-$, and H_2O in DNA and the high reactivity of the ·OH with various functional groups allow for the redox-mediated formation of the mutagenic OH-adducts and putatively nonmutagenic Fapy structures determined by GC-MS (Fig. 1).

The modified-base models (Fig. 3) revealed a >2-fold increase in total mean radical-induced oxidative damage in the IDC_m compared with the IDC. Moreover, the difference in standard deviations indicated that the IDC_m had greater base variation (diversity). Tumor cells have been shown to constitutively generate high concentrations of H_2O_2 (45). They also exhibit resistance to lysis by H_2O_2 (46) and likely possess specific antioxidant defenses (47), suggesting an ability to protect themselves from high concentrations of reactive oxygen species (4, 45–47). Thus, an explanation for the higher degree of radical damage inflicted on the IDC_m may be that metastatic cells are more deficient in antioxidant defenses in addition to having elevated levels of reactive oxygen species.

Of particular interest was the relationship between the $\log_{10}$(Fapy-A/8-OH-Ade) ratio and tumor size (Fig. 4). The $\log_{10}$ base ratios of the IDC were essentially unchanged over a broad range of tumor sizes, representing a tight cluster of values. The IDC_m ratios not only increased substantially with tumor size—favoring Fapy-A—but were also widely dispersed around the line, suggesting a substantially increased base diversity associated with metastatic tumor development and growth. The apparent shift in redox status (Fig. 1) favoring Fapy-A is difficult to understand (Fig. 4); however, it may tend to stabilize the delicate balance of

structural modifications in those subpopulations of DNA endowed with significant metastatic potential. The introduction of an oxygen atom at the 8-position of guanine has been shown to substantially change its electrostatic potential and impart a negative character that may alter DNA polymerase interactions, thus potentially modifying the fidelity of DNA replication (48). Hence, the apparent preference for the Fapy structure during the growth of metastatic tumors may prevent electrostatic changes from being introduced into DNA that threaten the viability of metastatic cells. The preference for the Fapy structure also suggests a reversion to conditions prevailing in the RMT in which the mean $\log_{10}$(Fapy-A/8-OH-Ade) was shown to be positive (24, 32).

DNA repair systems were considered as a possible explanation for the base changes; however, repair enzymes—e.g., glycosylases—show a diminished activity in breast and other tumor cells (31) and were also reported to have a similar specificity toward substrates containing OH-adducts and Fapy residues (19–21, 29). Accordingly, it seems unlikely that the substantial increase in $\log_{10}$(Fapy-A/8-OH-Ade) ratios (Fig. 4) can be significantly attributed to differential repair of the two types of modified base structures.

Additional insight was obtained by using FT-IR spectroscopy, which provided information on damage to the phosphodiester–deoxyribose backbone of the DNA as well as the base structure. A three-dimensional plot of PC scores was derived from FT-IR spectral correlations (Fig. 5). The greater diversity of the IDC_m group, noted earlier in connection with base concentrations and ratios, is also apparent in Fig. 5. The ·OH is known to react primarily with the double bonds of the bases, although it also abstracts hydrogens from deoxyribose leading to a series of reactions resulting in strand breaks (49). Both types of radical damage would be reflected in the FT-IR spectral properties associated with the IDC_m and IDC and would be expected to contribute to the spatial differences found between these DNA groups and the increased structural diversity of the IDC_m. The substantial diversity of the RMT is consistent with previous findings (32) in which the DNA of healthy women represented a nonrandom progression of damage attributed to the ·OH. The finding that both the IDC_m and the RMT have a greater diversity than the IDC (Fig. 5) is consistent with the notion that metastasis involves a reversion to DNA structural profiles found in normal tissue (32), as was also suggested by the apparent preference shown for the Fapy structure in relation to metastatic tumor growth (Fig. 4). Notwithstanding, the IDC_m would be expected to be enriched in mutagenic structures—e.g., base transversions—that are likely undetectable by the presently employed analytical techniques.

The three-dimensional plot reflects a high degree of structural specificity and represents over a million absorbance-wavenumber correlations. This specificity is evident in Fig. 6 in which less than 3% spectral difference exists between two samples (spheres) that are spatially close. The two IDC outliers are of additional interest. Given that the core IDC cluster had a high degree of pathologic homogeneity, it was expected that histologically divergent samples would fall outside the core cluster. Fig. 7 illustrates substantial spectral differences between the two outliers and the mean spectrum of the core IDC cluster, thereby supporting this perspective. Future research may confirm that PCA of FT-IR spectra is a promising technique with high structural specificity for discriminating DNA phenotypes in cancer diagnosis and prediction.

The present findings provide new understanding of factors governing metastatic transformations in the female breast and special emphasis is placed on the damaging effects of the ·OH on DNA. In this regard, an important factor in maintaining viable subpopulations of metastatic DNA in the breast would likely be the balance between the rate of damage and repair associated with both the base and deoxyribose structure (50, 51). Moreover, the substantial degree of base damage identified in the IDC_m may be closely linked to the activation or

Medical Sciences: Malins *et al.*

Proc. Natl. Acad. Sci. USA 93 (1996)   2563

augmentation of nuclear oncogenes (16–18) and the deregulation of tumor suppressor genes, such as p53 (52–54). The ·OH may also alter cellular proteins and carbohydrates critical for cell adhesion (3) and thus facilitate the development of metastasis. Considering that the ·OH damage is likely critical in the initiation and development of primary breast tumors (24, 32) and appears to play a pivotal role in metastasis, certain intervention strategies seem promising. These include regulation of redox shifts associated with mutagenic and related DNA damage, iron metabolism in relation to the catalytic conversion of H_2O_2 to the ·OH (55, 56), and control of redox cycling reactions of estrogens (9–12) and xenoestrogens (13–15) governing the generation of H_2O_2 and the ·OH. Antioxidant/reductant preparations that preferentially target the breast epithelium may be particularly promising in controlling the radical-induced damage. In this regard, vitamin C intake is reported to decrease breast cancer incidence in humans (57) and reduce estrogen-induced carcinogenesis in animals (58). The therapeutic effects of intervention could be monitored by using the discriminating analytical/statistical protocols described in this and previous reports (24, 32).

Evidence has been presented showing that the ·OH modification of DNA is intimately involved in the progression of breast tumors to the metastatic state and is likely an important etiologic factor contributing to the high degree of heterogeneity and diverse physiological properties characteristic of metastatic cell populations. In a broader sense, the findings strongly support the concept that conditions in the microenvironment have a profound effect on the ability of DNA to faithfully transcribe genetic information, a likely example being the radical modification of cancer-related genes. Future research, using the analytical techniques described, may provide an ability to identify critical metastatic changes in the DNA of a variety of transformed tissues prior to evidence at the cellular level.

1. Fidler, I. J. & Nicolson, G. L. (1991) in *The Breast: Comprehensive Management of Benign and Malignant Diseases*, eds. Bland, K. I. & Copeland, E. M., III (Saunders, Philadelphia,), pp. 395–408.
2. Kohn, E. C. & Liotta, L. A. (1995) *Cancer Res.* **55**, 1856–1862.
3. Kundu, N., Zhang, S. & Fulton, A. M. (1995) *Clin. Exp. Metastasis* **13**, 16–22.
4. Eskenazi, A. E., Pinkas, J., Whitin, J. C., Arguello, F., Cohen, H. J. & Frantz, C. N. (1993) *J. Natl. Cancer Inst.* **85**, 711–721.
5. Malins, D. C. (1993) *J. Toxicol. Environ. Health* **40**, 247–261.
6. Floyd, R. A. (1990) *Carcinogenesis* **11**, 1447–1450.
7. Imlay, J. A., Chin, S. M. & Linn, S. (1988) *Science* **240**, 640–642.
8. Zhao, M. J., Jung, L., Tanielian, C. & Mechin, R. (1994) *Free Radicals Res.* **20**, 345–363.
9. Roy, D., Floyd, R. A. & Liehr, J. G. (1991) *Cancer Res.* **51**, 3882–3885.
10. Sipe, H. J., Jr., Jordan, S. J., Hanna, P. M. & Mason, R. P. (1994) *Carcinogenesis* **15**, 2637–2643.
11. Han, X. & Liehr, J. G. (1994) *Cancer Res.* **54**, 5515–5517.
12. Han, X. & Liehr, J. G. (1995) *Carcinogenesis* **16**, 2571–2574.
13. Schraufstatter, I. U. & Jackson, J. H. (1992) in *Cellular and Molecular Mechanisms of Inflammation, Vol. 4*, eds. Cochrane, C. G. & Gimbrone, M. A., Jr. (Academic, New York), pp. 21–41.
14. Jackson, J. H., Schraufstatter, I. U., Hyslop, P. A., Vosbeck, K., Sauerheber, R. & Cochrane, C. G. (1987) *J. Clin. Invest.* **80**, 1090–1095.
15. Floyd, R. A., Watson, J. J., Harris, J., West, M. & Wong, P. K. (1986) *Biochem. Biophys. Res. Commun.* **137**, 841–846.
16. Kamiya, H., Miura, H., Murata-Kamiya, N., Ishikawa, H., Sakaguchi, T., Inoue, H., Sasaki, T., Masutani, C., Hanaoka, F., Nishimura, S. & Ohtsuka, E. (1995) *Nucleic Acids Res.* **23**, 2893–2899.
17. Kuchino, Y., Mori, F., Kasai, H., Inoue, H., Iwai, S., Mirua, K., Ohtsuka, E. & Nishimura, S. (1987) *Nature (London)* **327**, 77–79.
18. Cheng, K. C., Cahill, D. S., Kasai, H., Nishimura, S. & Loeb, L. A. (1992) *J. Biol. Chem.* **267**, 166–172.
19. Chetsanga, C. J. & Lindahl, T. (1979) *Nucleic Acids Res.* **6**, 3673–3684.
20. Chetsanga, C. J., Lozon, M., Makaroff, C. & Savage, L. (1981) *Biochemistry* **20**, 5201–5207.
21. Boiteux, S., O'Connor, T. R., Lederer, F., Gouyette, A. & Laval, J. (1990) *J. Biol. Chem.* **265**, 3916–3922.
22. Breimer, L. H. (1984) *Nucleic Acids Res.* **12**, 6359–6367.
23. Laval, J., Boiteux, S. & O'Connor, T. R. (1990) *Mutat. Res.* **233**, 73–79.
24. Malins, D. C., Holmes, E. H., Polissar, N. L. & Gunselman, S. J. (1993) *Cancer* **71**, 3036–3043.
25. Steenken, S. (1989) *Chem. Rev.* **89**, 503–520.
26. Klein, J. C., Bleeker, M. J., Saris, C. P., Roelen, H. C. P. F., Brugghe, H. F., van den Elst, H., van der Marel, G. A., van Boom, J. H., Westra, J. G., Kriek, E. & Berns, A. J. M. (1992) *Nucleic Acids Res.* **20**, 4437–4443.
27. Koch, K. S., Fletcher, R. G., Grond, M. P., Inyang, A. I., Lu, X. P., Brenner, D. A. & Leffert, H. L. (1993) *Cancer Res.* **53**, 2279–2286.
28. Dee, D. & Baur, M. E. (1974) *J. Chem. Phys.* **60**, 541–559.
29. Tchou, J., Kasai, H., Shibutani, S., Chung, M.-H., Laval, J., Grollman, A. P. & Nishimura, S. (1991) *Proc. Natl. Acad. Sci. USA* **88**, 4690–4694.
30. Chetsanga, C. J. & Grigorian, C. (1985) *Proc. Natl. Acad. Sci. USA* **82**, 633–637.
31. Pero, R. W., Roush, G. C., Markowitz, M. M. & Miller, D. G. (1990) *Cancer Detect. Prev.* **14**, 555–561.
32. Malins, D. C., Polissar, N. L., Nishikida, K., Holmes, E. H., Gardner, H. S. & Gunselman, S. J. (1995) *Cancer* **75**, 503–517.
33. Morgan-Parkes, J. H. (1995) *Am. J. Roentgenol.* **164**, 1075–1082.
34. Symmans, W. F., Liu, J., Knowles, D. M. & Inghirami, G. (1995) *Hum. Pathol.* **26**, 210–216.
35. Saran, M. & Bors, W. (1990) *Radiat. Environ. Biophys.* **29**, 249–262.
36. Dunn, B. P., Black, J. J. & Maccubbin, A. (1987) *Cancer Res.* **47**, 6543–6548.
37. Dizdaroglu, M. & Gajewski, E. (1990) *Methods Enzymol.* **186**, 530–544.
38. Sutherland, G. B. B. M. & Tsuboi, M. (1957) *Proc. R. Soc. A. Math. Phys. Sci.* **239**, 446–463.
39. Parker, F. S. (1983) *Applications of Infrared, Raman, and Resonance Raman Spectroscopy in Biochemistry* (Plenum, New York), pp. 349–398.
40. Nowell, P. C. (1976) *Science* **194**, 23–28.
41. Sierra, A., Lloveras, B., Castellsagué, X., Moreno, L., García-Ramirez, M. & Fabra, A. (1995) *Intl. J. Cancer* **60**, 54–60.
42. Steeg, P. S., Bevilacqua, G., Sobel, M. E. & Liotta, L. A. (1991) *Boundaries Between Promotion and Progression During Carcinogenesis* (Plenum, New York), pp. 355–361.
43. Olinski, R., Zastawny, T., Budzbon, J., Skokowski, J., Zegarski, W. & Dizdaroglu, M. (1992) *FEBS Lett.* **309**, 193–198.
44. Frenkel, K. & Chrzan, K. (1987) *Carcinogenesis* **8**, 455–460.
45. O'Donnel-Tormey, J., DeBoer, C. J. & Nathan, C. F. (1985) *J. Clin. Invest.* **76**, 80–86.
46. Nathan, C. F., Arrick, B. A., Murray, H. W., DeSantis, N. M. & Cohn, Z. A. (1981) *J. Exp. Med.* **153**, 766–782.
47. Szatrowski, T. P. & Nathan, C. F. (1991) *Cancer Res.* **51**, 794–798.
48. Aida, M. & Nishimura, S. (1987) *Mutat. Res.* **192**, 83–89.
49. Von Sonntag, C., Hagen, U., Schön-Bopp, A. & Schulte-Frohlinde, D. (1981) *Adv. Rad. Biol.* **9**, 110–142.
50. Frenkel, K. (1992) *Pharmacol. Ther.* **53**, 127–166.
51. Demple, B. & Harrison, L. (1994) *Annu. Rev. Biochem.* **63**, 915–948.
52. Coles, C., Condie, A., Chetty, U., Steel, C. M., Evans, H. J. & Prosser, J. (1992) *Cancer Res.* **52**, 5291–5298.
53. Thompson, A. M., Anderson, T. J., Condie, A., Prosser, J., Chetty, U., Carter, D. C., Evans, H. J. & Steel, C. M. (1992) *Intl. J. Cancer* **50**, 528–532.
54. Peller, S., Halevy, A., Slutzki, S., Kopilova, Y. & Rotter, V. (1995) *Mol. Carcinog.* **13**, 166–172.
55. Aruoma, O. I., Halliwell, B. & Dizdaroglu, M. (1989) *J. Biol. Chem.* **264**, 13024–13028.
56. Gutteridge, J. M. C. & Quinlan, G. J. (1993) *Biochim. Biophys. Acta* **1156**, 144–150.
57. Block, G. (1991) *Am. J. Clin. Nutr.* **53**, 2705–2825.
58. Liehr, J. G. & Wheeler, W. J. (1983) *Cancer Res.* **43**, 4638–4642.